



Directed energy deposition process optimization and factor interaction analysis by response surface methodology

Jun-Ru Qiu¹ · Yu-Xiang Chen¹ · Yi-Kai Hwang¹ · Wei-Ling Chang¹ · Sheng-Jye Hwang¹

Received: 24 January 2024 / Accepted: 19 April 2024 / Published online: 1 May 2024
© The Author(s), under exclusive licence to Springer-Verlag London Ltd., part of Springer Nature 2024

Abstract

The purpose of this study is to optimize the critical parameters of the directed energy deposition (DED) process using the response surface methodology (RSM) and central composite design (CCD). The experiments investigate the influence of three key process factors, namely laser power, powder feed rate, and scanning speed, on deposition efficiency, deposition rate (DR), and porosity. Additionally, through analysis of variance (ANOVA), the significant factors and interaction effects are identified, and predictive models are developed for quality prediction. The research successfully optimizes the process parameters, which are validated through the fabrication of geometric components, specifically thin-walled nozzles. The study introduces innovative approaches such as “plunge-cutting toolpath” and “hybrid laser head lift height (Z-offset) method” to address the challenges associated with complex geometries. Additionally, the reliability and practicality of the optimized process parameters are confirmed.

Keywords Directed energy deposition · Response surface methodology · Central composite design · Microstructural properties · Toolpath planning

1 Introduction

The DED process involves transporting powder material to the substrate through an inert gas, typically argon (Ar) or helium (He). The laser head focuses on the desired position, emitting a laser beam from its center to heat the powder material at that location. This process results in the melting of the material above the substrate, which cools and solidifies into the desired shape. According to research conducted by the British Welding Institute [1], the DED process is ten times faster than the PBF process in terms of manufacturing speed and has a cost that is five times lower than that of the PBF process. Its advantages include the ability to repair workpieces, manufacture products with mixed material structures, and create large workpieces. These advantages make DED a highly desirable manufacturing process.

Research in the field of DED can be broadly classified into three directions. Firstly, the optimization of process

parameters through experimental design methods. Secondly, the advancement of DED technology to manufacture products using different toolpath planning methods and study the product's appearance. Lastly, research on composite materials by mixing powders or stacking two different materials alternately to investigate the mechanical properties and microstructural characteristics of the product.

In the field of experimental design and process parameter optimization, various studies have been conducted. For example, Guo et al. [2] used the central composite design (CCD) method in the response surface methodology (RSM) to perform experiments with four factors and five levels. The study aimed to explore the interaction of factors on surface roughness, deposition width, and melting area of rectangular geometry to understand the influence of process parameters on geometric characteristics. Ansari et al. [3] conducted two-factor and three-level experiments using the central composite design method, with energy density and powder density as control factors, to explore the most objective performance of process parameters through single-track deposition. They studied the deposition after wire cutting and observed the microstructure of the deposition zone (DZ), heat-affected zone (HAZ), and dilution zone to interpret the influence of process

✉ Sheng-Jye Hwang
jimpp1@mail.ncku.edu.tw

¹ Department of Mechanical Engineering, National Cheng Kung University, No.1, University Road, Tainan 701401, Taiwan

parameters on the deposition product from a microscopic perspective. Svetlizky et al. [4] used Al5083 as the experimental material and applied the central composite design method to carry out the DED double-track deposition experiment to study the influence of process factors on deposition height and dilution rate. They explored the interaction relationship between factors using the second-order analysis of variance (ANOVA) method and established a second-order regression model. The study found that the powder feed rate had a significant impact on the deposition height, and the interaction between powder feed rate and hatching space (HS) showed a significant effect. Lastly, Fujishima et al. [5] studied the influence of different process factors on the deposition results during multi-layer and single-track deposition. They used a high-speed camera to record the deposition process and observed changes in the melt pool between different parameters. The study found that improper parameter selection could cause product defects, such as incomplete melting due to low laser power, leading to cracks caused by unmelted powder particles wrapped in the deposited layer, and excessive energy density causing local vaporization to form pores called keyholes.

In order to industrialize the DED process, toolpath planning is an important area of research. Ribeiro et al. [6] investigated the effects of different deposition paths on the geometric appearance, microhardness, and microstructure of the product. Four toolpaths were used: linear, zigzag, contour, and chessboard. Two sets of experiments were conducted with different overlapping ratios. The results showed that the contour toolpath produced the best geometric structure and surface roughness performance. However, the deep valley effect was influenced by different overlapping ratios. Too small an overlap ratio resulted in deeper valleys and degraded surface roughness, while too large an overlap ratio increased material consumption and decreased cladding efficiency. Kaji et al. [7] studied the feasibility of additive manufacturing with multi-axis machining. The research verified the possibility of multi-axis machining by manufacturing a hollow suspended hemisphere and preventing deposition from being affected by gravity, viscous force, and surface tension. Oh et al. [8] used toolpath planning to repair damaged workpieces through the DED process. The feasibility and method of repairing workpieces with DED were verified, and the effects of thermal stress on the mechanical properties of the repaired product were observed. Li et al. [9] studied the influence of different groove geometries on DED process repair by grooving the damaged part before repair. The results showed that the trapezoidal groove enabled the laser head to be filled layer by layer, resulting in a slightly lower tensile stress of the repaired parts than that of the original material. However, the DED process still

caused cracks when the repaired part cooled and shrank after repair, which further deteriorated the repairing effect.

When it comes to material properties, composite materials are increasingly being used in DED, and research on their structural and mechanical properties is emerging as a key area. In a study by Aydogan et al. [10], two different powders were mixed using the DED process, and mechanical properties were compared between products with different mixing ratios. The products were also heat-treated to assess changes in their microstructure. Results indicated that an increase in the proportion of nickel-based (Ni) material led to reduced cracks between products and a more uniform structure after heat treatment. In another study, Melzer et al. [11] used stainless steel SS316L and nickel-based superalloy IN718 for composite deposition. During the DED process, the material was alternately deposited into a three-dimensional rectangular workpiece, which was then subjected to tensile and miniaturized compact tension (MCT) tests. As the melting points of the two materials were different, different process parameters were used during manufacturing. When SS316L was deposited on IN718, high laser power caused the materials to melt simultaneously, resulting in good bonding at the deposition interface. Conversely, low laser power when depositing IN718 on SS316L led to poor bonding due to insufficient melting of the existing SS316L layer. Tensile and MCT tests showed that the interface layer with better bonding performed better overall. Lastly, Wei et al. [12] investigated the influence of different deposition methods on the mechanical properties and microstructure of a product, using copper alloy (Cu10Sn), stainless steel (SS316L), and tungsten (W) for deposition using the PBF method. The study found that direct deposition or mixed materials led to incomplete melting, causing unmelted powders to become trapped and leading to cracks and reduced mechanical strength. However, using nickel-rich stainless steel as an intermediate transition layer led to better bonding, as nickel-based metals have higher wettability and diffusion coefficients that enable better material combination.

In this study, we utilized the central composite design method to establish an experimental parameter table and designed a 3-factor 5-level experiment. Initially, a single-track experiment was conducted to confirm the single-track width and height of each set of process parameters. Next, the cladding efficiency, deposition rate, and porosity were selected as the quality factors to carry out multi-layer and multi-track experiments. The experimental results were analyzed by two-way ANOVA to identify significant factors and their interactions. Additionally, a regression analysis method was used to establish a regression model, enabling users to predict process quality, avoid unnecessary waste, and reduce costs.

To validate the optimization results of the DED process factors, we also conducted path planning research using NX

CAM software. Specifically, we designed the nozzle geometry as the target workpiece and employed different toolpath planning methods. Using the optimal combination of process parameters obtained in the response surface experiments, we verified the reliability and formability of the parameters and successfully produced a geometric workpiece with an overhanging angle and torsion.

2 Materials and methods

2.1 Equipment and materials

The equipment used in this research for the DED system is displayed in Fig. 1. The laser head was installed on the Tongtai TMV-710A machine tool which is capable of five-axis simultaneous movement and equipped with a double rotary table. The laser system utilized the IPG-YLS-3000 fiber laser with a maximum power of 3000 W and a wavelength of 1070 nm. The laser spot diameter was 3 mm, and it had a flat-top energy distribution. The Precitec YC30 laser head used was a coaxial four-way powder feeding type with a hub that could adjust the laser focus position. The GTV PF 2/2 LC powder feeder was used to transport metal powder to the laser head. It included a rotating powder disk, and the transporting unit was measured in rpm, with 1 rpm equivalent to 10.08 g/min. Argon gas was used for powder supply and laser head protective gas.

Both the powder and substrate materials used in this study were nickel-based superalloy IN 718, a material known for its outstanding properties at high temperatures (up to 980 °C), as well as its excellent oxidation and corrosion resistance. It is widely used in the aeronautical sector [13]. The substrate geometry used in this study was L100 x W100 x H15 mm³. The IN 718 powder was generated by

gas atomization, and its particle size distribution range was 53–150 μm. The detailed analysis results of the particle size distribution are displayed in Tables 1, 2, and 3.

2.2 Design of RSM experiment

The response surface method is widely used in research fields such as electronics, machinery, agriculture, material science, food science, and industrial process improvement. It aids researchers in providing solutions to problems such as optimal product design, process improvement, and system optimization in scientific systems or industrial processes.

In this study, response surface methodology (RSM) was employed as the experimental design method, which encompasses various experimental design techniques. Central composite design (CCD) was chosen for experimental design in this study. CCD consists of corner points, axial points, and center points. Corner points represent experimental combinations generated by setting control factors at different levels in the experimental design. Axial points are selected to be higher and lower than the levels of control factors. To achieve rotatability in the experimental design, experiments are conducted at distances α from the center point (both ends) along the axis, where α is defined as follows:

$$\alpha = \sqrt[4]{F} \quad (1)$$

In this process, F represents the number of experiments in the corner point design, while the center point experiment consists of the median level of each control factor, serving as the midpoint of the control factor levels in the experimental design. To enhance experimental precision, center point experiments are typically repeated to reduce experimental errors.

The experimental procedure for response surface methodology is as follows: (1) Select control factors and define the experimental quality, (2) determine the levels of variation for control factors, (3) design an orthogonal array, (4) conduct experiments according to the orthogonal array, (5) record the quality of experimental results, (6) analyze the experimental results to determine the optimal combination of factors, and (7) perform verification experiments.

To explore the interaction effects of process parameters, laser power, powder feed rate, and scanning speed were chosen as control factors, and a multi-layer geometry with

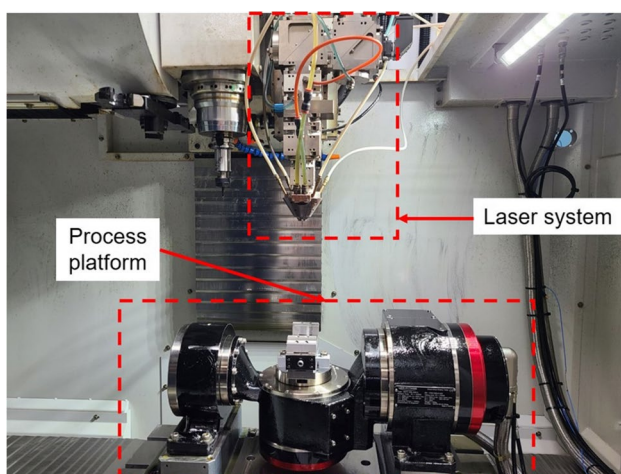


Fig. 1 DED system

Table 1 IN 718 powder particle size distribution

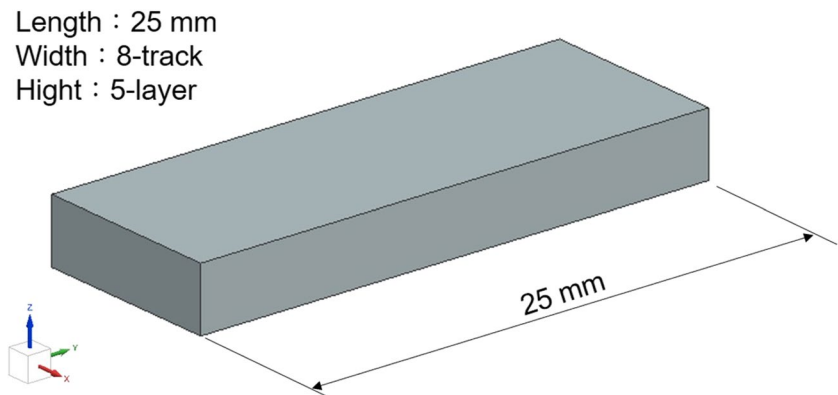
Item	Result	Specification	Unit
D_{10}	65.64	53–150	μm
D_{50}	89.78		μm
D_{90}	123.76		μm

Table 2 IN 718 powder composition

Element	Al	B	Co	Cr	Cu	Fe	Mn	Mo	
Testing method	ICP-OES								
Result	0.5404	ND	0.0485	17.78	0.0276	Bal	0.0537	3.0574	
Specification	Min	0.2	0	0	17	0	Bal	0	2.8
	Max	0.8	0.006	1	21	0.3	Bal	0.35	3.3
Unit	wt%								

Table 3 IN 718 powder composition

Element	Nb	Ni	P	Si	Ta	Ti	C	S
Testing method	ICP-OES						C/S Analyzer	
Result	5.1372	52.514	0.0026	0.0894	0.0046	1.0041	0.0316	0.0013
Specification	Min	4.75	50	0	0	0	0.65	0
	Max	5.5	55	0.015	0.35	0.05	1.15	0.08
Unit	wt%							

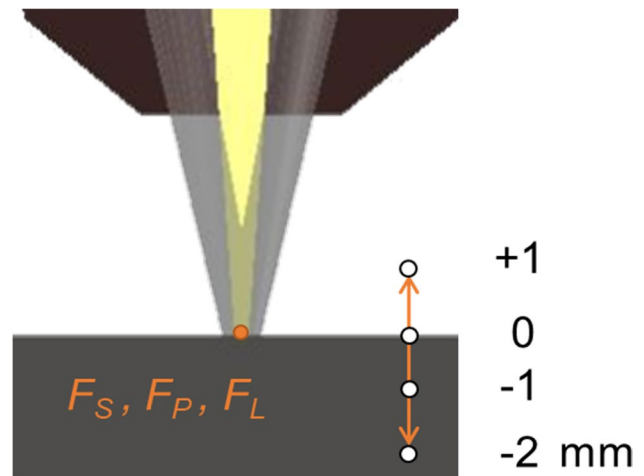
Fig. 2 Schematic of RSM experiment workpiece

8 tracks and 5 layers was used as an experimental product (as shown in Fig. 2). The purpose was to investigate the influence of different parameter combinations on three-dimensional products and the interaction relationships between parameters.

In the DED process, there are numerous factors that can significantly impact product quality. To eliminate the influence of these factors on experimental results, this study fixed the following parameters:

(1) Laser defocus distance

The setting of the laser defocus distance is the relative position of the laser focus (F_L) and deposition surface (F_S) under the premise that the powder focus (F_P) and F_S are the same. As shown in the Fig. 3, positive/negative indicates the position above/below the deposit, while the value represents the distance. After conducting research, it was discovered that the deposition process could be repaired when the laser focus was located below the substrate. This enabled the surface of the workpiece to be filled to the same height. As a

**Fig. 3** Schematic of laser defocus distance

result, the laser focus distance was fixed at 2 mm below the substrate in this study.

(2) Overlap ratio

During the DED process of multi-track geometric workpieces, tracks tend to overlap each other. As shown in the Fig. 4, the overlapping ratio can be adjusted by changing the hatching space distance. The formula for calculating the overlap ratio is as follows:

$$Overlap\ ratio = \frac{W - H}{W} 100\% \tag{2}$$

where W is the width of a single track, and H is the hatching space between the track and the center of the track. In this study, the overlap ratio is fixed at 60%.

(3) Rising distance of laser head (Z-offset)

When processing a three-dimensional workpiece with a multi-layer geometry, thermal deformation often occurs, causing the original deposition layer to shrink as the processing layers are stacked upwards. This results in the deposition height being below the set value, as shown in the Fig. 5.

The definition of Z-offset is shown as follows:

$$Z - offset = H_1 \cdot \frac{H_2}{H_1} = H_1 \cdot D_h = H_1 \cdot (1 - \delta) \tag{3}$$

Fig. 4 Schematic of overlap ratio

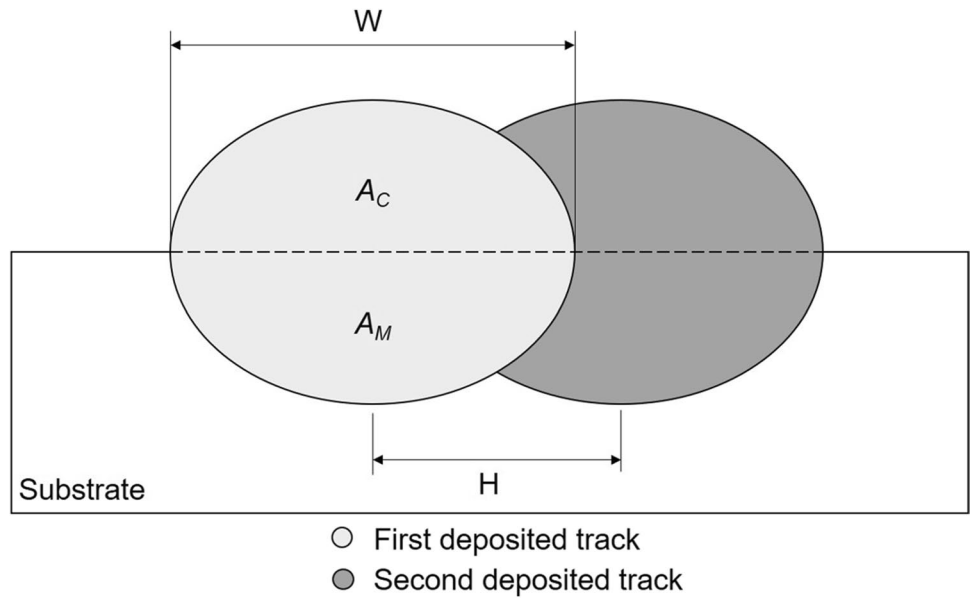


Fig. 5 Schematic of thermal deformation

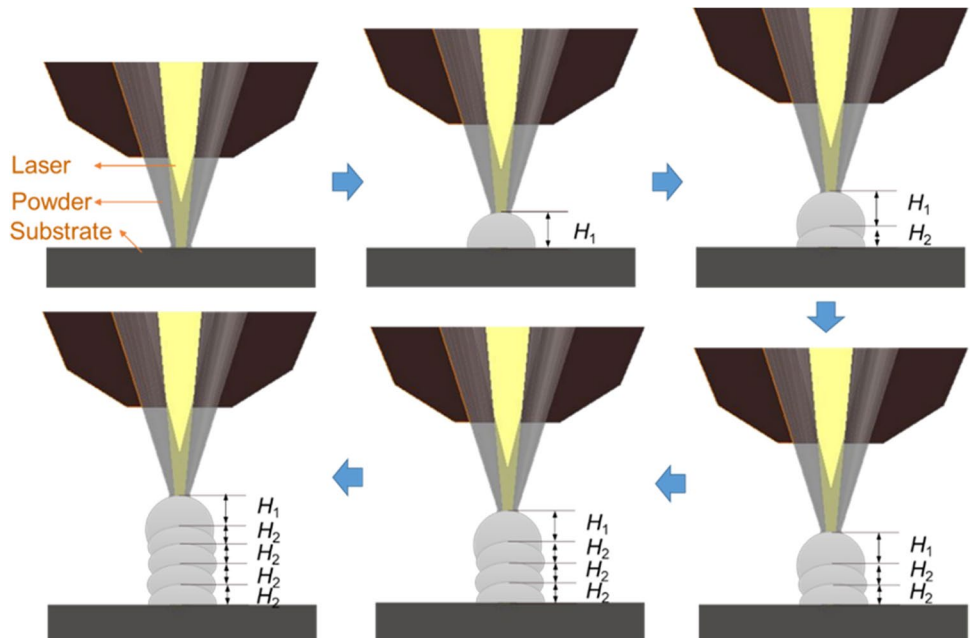


Table 4 Control factors and its level values

Notation	Factor	Factor levels				
		-1.633	-1	0	1	1.633
A	Laser power (W)	1000	1200	1400	1600	1800
B	Powder feed rate (rpm)	0.3	0.5	0.7	0.9	1.1
C	Scanning speed (mm/s)	11	12	13	14	15

Table 5 Setting values of fixed factors

Notation	Fixed factor	Data
A	Overlap ratio (%)	60
B	Z-offset (%)	50
C	Laser defocus (mm)	-2
D	Number of tracks	8
E	Number of layers	5

Table 6 Central composite design

Run	A Laser power (W)	B Powder feed rate (rpm)	C Scanning speed (mm/s)
1	1000	0.7	13
2	1200	0.5	12
3	1200	0.9	14
4	1200	0.9	12
5	1200	0.5	14
6	1400	0.7	13
7	1400	0.7	13
8	1400	0.7	13
9	1400	0.7	13
10	1400	0.7	13
11	1400	0.7	13
12	1400	0.7	11
13	1400	0.7	15
14	1400	1.1	13
15	1400	0.3	13
16	1600	0.5	14
17	1600	0.9	14
18	1600	0.9	12
19	1600	0.5	12
20	1800	0.7	13

$$D_h = \frac{H_2}{H_1}$$

$$\delta = \frac{H_1 - H_2}{H_1} = 1 - D_h$$

while H_1 is the height of the first layer. H_2 is the height of the first layer after thermal deformation. D_h is the reduction degree of the height of the old layer when heated. δ is the shrinkage of the height of the old layer. According to previous research findings: “The shrinkage of the old layer height caused by thermal deformation is the same as the single layer deposition dilution d ,” so this study set the laser head lift height at 50%.

After introducing the control and fixed factors, the experimental design was conducted using Minitab, an experimental design software. The central composite design method was employed to establish a response surface experiment with 3 factors and 5 levels. The design is presented in Tables 4, 5 and 6.

2.3 Product properties

In the DED process, several problems and challenges remain to be addressed, including inadequate cladding efficiency, internal pores in the workpiece, and suboptimal surface roughness. Hence, this study focuses on improving product quality by optimizing cladding efficiency, deposition rate, and porosity using the response surface experiment method. This approach aims to identify the interaction between process parameters and determine the optimal combination of process parameters.

The following sections will introduce the definition of each product quality in detail:

(1) Cladding efficiency (CE)

Cladding efficiency is defined as the ratio of the actual weight of the powder that is successfully deposited on the workpiece to the overall weight change of the substrate before and after processing. It indicates how effectively the powder is deposited on the workpiece during processing. The calculation formula of cladding efficiency is as follows:

$$CE = \frac{W_{clad}}{W_{feed}} \cdot 100\% \tag{4}$$

where W_{clad} is the increase of substrate weight after cladding and W_{feed} is the weight of input powder, which is

equal to the product of powder feed rate and cladding time.

(2) Deposition rate (*DR*)

If cladding efficiency is the product quality set for the cost of material, then deposition rate is the target set for the cost of time. In this study, deposition rate is defined as the weight of powder deposited on the substrate per unit time. The formula of calculating the deposition rate is as follows:

$$DR = \frac{W_{clad}}{t} \cdot 60 \tag{5}$$

where the unit of *DR* is g/min and *W_{clad}* is the increase of substrate weight after cladding. *t* is the processing time (Unit: sec).

(3) Porosity (*P_t*)

In the DED process, pores are a critical product quality that can significantly affect the mechanical properties of the workpiece. Pores can form due to various reasons such as the entrapment of transport gas during the solidification process of the molten pool, or when the energy density per unit area is too high due to inappropriate process parameter selection, resulting in vaporization of the material and the formation of keyholes. These pores can have a significant negative impact on mechanical properties such as tensile strength and microhardness of the product. Therefore, reducing porosity is a crucial quality target for DED process optimization. As show in Fig. 6, optical microscope images were captured, and Image J software was employed to calculate pore areas in the specimen cross-sections.

The formula of porosity is as follows:

$$P_t = \frac{\sum_{i=1}^n A_i}{A_C + A_M} \cdot 100\% \tag{6}$$

where $\sum_{i=1}^n A_i$ is sum of cross-section area of pores, *A_C* is the cross-section area of cladded material, and *A_M* is the cross-section area of melt pool.

2.4 Optimization of RSM experiment

This study utilizes the response surface experiment method for multi-objective quality optimization proposed by Derringer and Suich [14] in 1980. Their procedure employs desirability functions to combine multiple qualities, where each response value *y_i* is converted into a desirability function *d_i*, with $0 < d_i < 1$. The desirability function is used to optimize multiple response surfaces and can be calculated using the weight geometric mean, which is defined mathematically as follows:

$$D = (d_1 \cdots d_m)^{\frac{1}{m}} \tag{7}$$

where *m* is the number of response experiments, and the desirability function depends on the solution target, which is the same as the Taguchi experiment method. It is divided into three categories: larger-the-better, smaller-the-better, and nominal-the-best. The mathematical formula is defined as follows:

(1) Larger-the-better

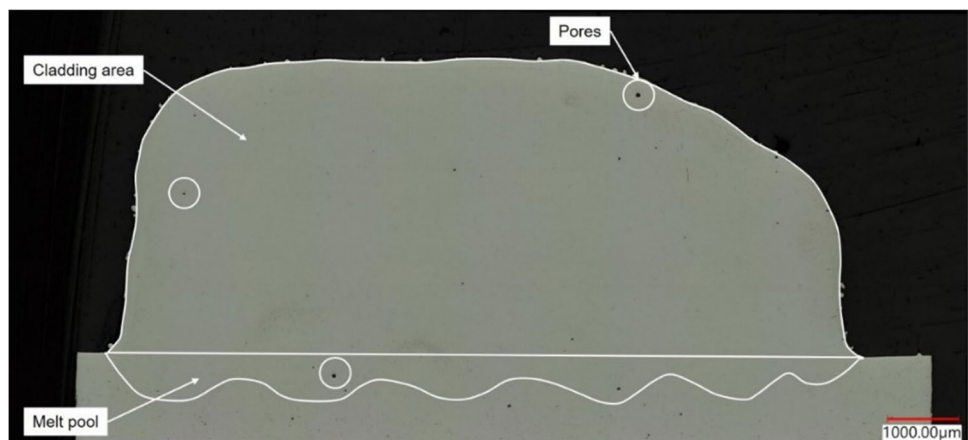
When the ideal target of the response value is the maximum response value, the desirability function can be calculated by the following mathematical formula:

$$d = \begin{cases} 0 & y < L \\ \left(\frac{y-L}{T-L}\right)^r & L \leq y \leq T \\ 1 & y > T \end{cases} \tag{8}$$

(2) Smaller-the-better

When the ideal target of the response value is the minimum response value, the desirability function can be calculated by the following mathematical formula:

Fig. 6 Cross-section image



$$d = \begin{cases} 1 & y < T \\ \left(\frac{U-y}{U-T}\right)^r & T \leq y \leq U \\ 0 & y > U \end{cases} \quad (9)$$

(3) Nominal-the-best

When the ideal target of the response value is between the upper and lower limits of the maximum and minimum response values, the desirability function can be calculated by the following mathematical formula:

$$d = \begin{cases} 0 & y < L \\ \left(\frac{y-L}{T-L}\right)^{r_1} & L \leq y \leq T \\ \left(\frac{U-y}{U-T}\right)^{r_2} & T \leq y \leq U \\ 0 & y > U \end{cases} \quad (10)$$

where T represents the target response value, U represents the maximum upper limit of the response value, and L represents the minimum lower limit of the response value. The variable r represents the relative importance of each quality, where $r=1$ represents equal importance among the different qualities, and $r>1$ means that the closer the response value is to the target value, the more important it is. Conversely, when $0 < r < 1$, it means that the response value is less important. In this study, the importance of each quality is set to 1, assuming equal importance for all qualities.

Based on the above sections, this study has set the larger-the-better criterion for cladding efficiency and deposition rate, and the smaller-the-better criterion for porosity. The experiment results were optimized using Minitab software.

3 Results and discussion

The target workpiece was deposited according to the central composite design experiment table. To minimize the error in experimental results caused by heat accumulation during the deposition process, test pieces were deposited on two substrates alternately during processing. The experimental results are shown in the Fig. 7 and Table 7.

3.1 Cladding efficiency

As shown in Table 8 and Fig. 8, based on the variance of the range of change, the significant degree of influence is as follows: powder feed rate (B) > laser power (A) > scanning speed (C).

As laser power increases, the energy density also increases, which enhances the laser's ability to melt powder per unit area. This leads to the melting of more powder materials and an improvement in cladding efficiency. Powder amount is the most significant factor affecting cladding efficiency. When the powder feed rate is increased, the cladding efficiency decreases significantly. When the powder supply is minimal, the powder material per unit area absorbs more energy, and the powder material can absorb energy uniformly and deposit on the substrate. However, when the powder supply is increased beyond a certain point, the laser's melting ability becomes limited, and too much powder material sprayed cannot effectively absorb the laser energy. Consequently, the powder material is not completely deposited on the substrate, resulting in a decrease in cladding efficiency. Table 7 shows that the highest cladding efficiency is achieved when the powder amount is 0.3 rpm (Run 15). However, this small powder amount also leads to a smaller workpiece size, which negatively impacts the geometric structure. While scanning speed is a less significant controlling factor, the deposition efficiency is mainly

Fig. 7 Image of RSM experiment: **a** run 1–10 and **b** Run 11–20

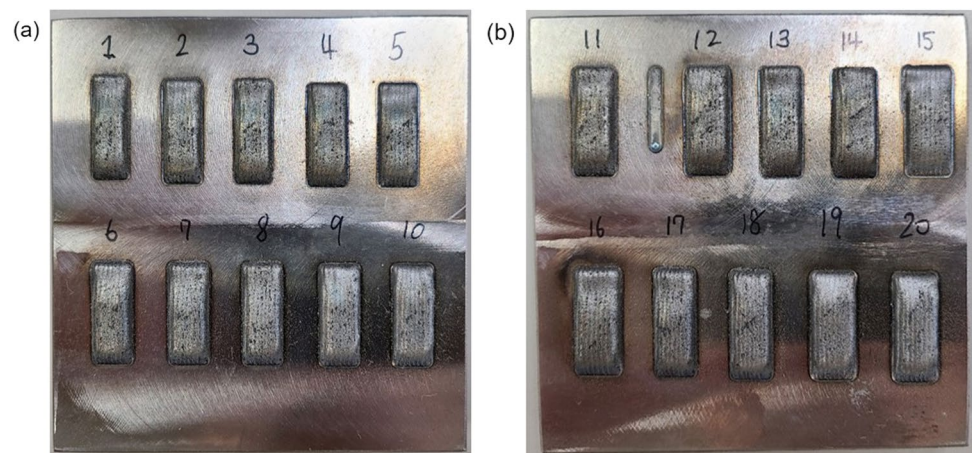


Table 7 Results of RSM experiment

Run	A Laser power (W)	B Powder feed rate (rpm)	C Scanning speed (mm/s)	Cladding efficiency (%)	Deposition rate (g/min)	Porosity (%)
1	1000	0.7	13	44.43%	3.13	1.003%
2	1200	0.5	12	50.13%	2.53	0.280%
3	1200	0.9	14	41.94%	3.80	0.512%
4	1200	0.9	12	41.42%	3.76	0.513%
5	1200	0.5	14	55.17%	2.78	1.274%
6	1400	0.7	13	48.31%	3.41	0.759%
7	1400	0.7	13	47.83%	3.38	0.199%
8	1400	0.7	13	48.80%	3.44	0.272%
9	1400	0.7	13	46.87%	3.31	0.345%
10	1400	0.7	13	45.90%	3.24	0.135%
11	1400	0.7	13	48.31%	3.41	0.141%
12	1400	0.7	11	47.47%	3.35	0.159%
13	1400	0.7	15	48.11%	3.39	0.686%
14	1400	1.1	13	40.74%	4.52	0.219%
15	1400	0.3	13	72.98%	2.21	0.045%
16	1600	0.5	14	58.79%	2.96	0.151%
17	1600	0.9	14	45.97%	4.17	0.247%
18	1600	0.9	12	44.56%	4.04	0.146%
19	1600	0.5	12	52.01%	2.62	0.012%
20	1800	0.7	13	48.31%	3.41	0.042%
Avg	-	-	-	48.90%	3.34	0.357%

Table 8 The average value of cladding efficiency at each level (unit: %)

Unit: %	A Laser power	B Powder feed rate	C Scanning speed
Level - α	44.43%	72.98%	47.47%
Level -1	47.16%	54.02%	47.03%
Level 0	49.53%	47.43%	49.25%
Level + 1	50.33%	43.47%	50.47%
Level + α	48.31%	40.74%	48.11%
Range	5.90%	32.24%	3.44%

dependent on the interaction between laser power and powder supply amount, and therefore, scanning speed does not have a direct impact.

The ANOVA analysis of cladding efficiency is presented in Table 9. The results indicate that the powder feed rate has the highest F value of 36.9703, suggesting that it is the most significant factor affecting cladding efficiency. On the other hand, the F values for laser power and scanning speed are 1.4841 and 0.8995, respectively, indicating that their influence is not as significant. Regarding the factor interactions, there is no apparent interaction among the three

factors. However, the F value of the powder feed rate and scanning speed interaction is the highest, which is related to how the deposition efficiency is calculated in this study. Since the scanning speed affects the processing time, and the processing time affects the total powder supply, the interaction among the three factors has the most significant impact on cladding efficiency.

3.2 Deposition rate

As shown in Table 10 and Fig. 9, based on the variance of the range of change, the significant degree of influence is as follows: powder feed rate (B) > laser power (A) > scanning speed (C).

As the powder feed rate increases, the deposition rate gradually increases. The deposition rate is mainly affected by the powder feed rate and processing time. Therefore, when the powder feed rate increases, more powder enters the molten pool per unit time. The workpiece can obtain more material. According to the research of Svetlizky et al. [4], the amount of powder feed rate has a significant impact on the height of the workpiece. The main reason is that the powder feed rate affects the amount of material entering the molten pool. In turn, the molten pool can obtain more materials so that the workpiece can grow higher. In addition,

Fig. 8 Response graph of cladding efficiency

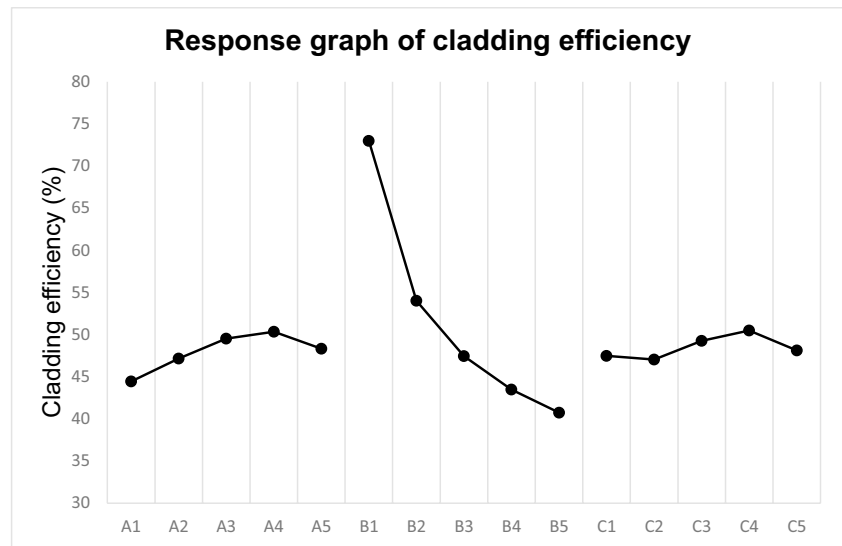


Table 9 ANOVA of cladding efficiency

Factor	SS	DF	MS	F value
A	0.002709	1	0.002709	1.4841
B	0.067485	1	0.067485	36.9703
C	0.001642	1	0.001642	0.8995
AB	0.000035	1	0.000035	0.0192
AC	0.000086	1	0.000086	0.0471
BC	0.001223	1	0.001223	0.6700
Error	0.023730	13	0.001825	-
Total	0.096452	19	-	-

Table 10 The average value of deposition rate at each level (unit: g/min)

Unit: g/min	A Laser power	B Powder feed rate	C Scanning speed
Level - α	3.135	2.2069	3.3495
Level -1	3.217	2.723	3.237
Level 0	3.365	3.347	3.345
Level +1	3.449	3.944	3.430
Level + α	3.409	4.517	3.3947
Range	0.314	2.310	0.193

as the laser power increases, the deposition rate is slightly affected. The main reason is that the laser power has the ability to melt powder at all levels, as shown in the experimental results of run 14 in the Table 7. When the laser power is fixed at 1400 W, the larger the powder feed rate, the better the deposition rate. Therefore, the increase in laser power is helpful to the melting ability of the material, but the powder feed rate is still the most significant factor affecting the

deposition rate. The scanning speed has the least significant effect on the deposition rate; the main reason is that in this study, the change of scanning speed has little difference in the processing time. When the scanning speed increases, the amount of powder supplied per unit time decreases instead. In the case of small processing time changes, the reduction of powder feed rate has a more significant impact on the deposition rate.

The ANOVA analysis of the deposition rate is shown in the Table 11; the *F* value of the powder feed rate is as high as 728.0751, which means that its influence on the deposition rate is extremely significant. There is an interaction between laser power and powder feed rate (AB); the main reason is that the laser power affects the powder melting ability, and the two must cooperate with each other. There is also an interaction between powder feed rate and scanning speed (BC). The scanning speed not only affects the powder density, but also variance the overall processing time, resulting in changes in the total powder feed rate. Therefore, the coordination between the powder feed rate and the scanning speed is also very important.

3.3 Porosity

As shown in Table 12 and Fig. 10, Based on the variance of the range of change, the significant degree of influence is as follows: laser power (A) > scanning speed (C) > powder feed rate (B).

The laser power is the most significant factor, and the main reasons are as follows: (1) When the laser power is too large, the energy density will be too high, which will increase the energy per unit area, cause the material to vaporize locally, and then generate pores. This phenomenon is called the keyhole phenomenon. (2) During processing, when the inert gas used to transport the powder

Fig. 9 Response graph of deposition rate

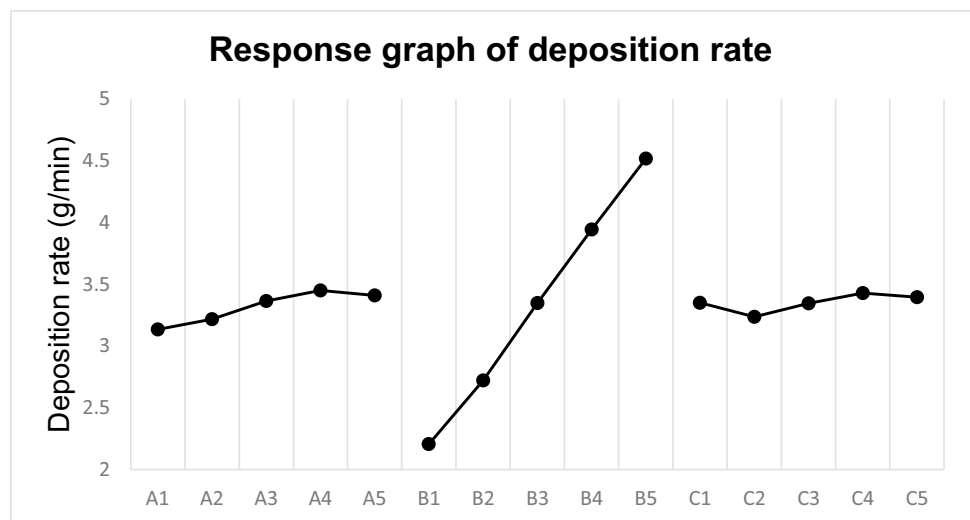


Table 11 ANOVA of deposition rate

Factor	SS	DF	MS	F value
A	0.14184	1	0.1418	18.3712
B	5.62130	1	5.6213	728.0751
C	0.05362	1	0.0536	6.9449
AB	0.01736	1	0.0174	2.2485
AC	0.00358	1	0.0036	0.4637
BC	0.02210	1	0.0221	2.8624
Error	0.100370	13	0.0077	-
Total	5.96018	19	-	-

Table 12 The average value of porosity at each level (unit: ‰)

Unit: ‰	A Laser power	B Powder feed rate	C Scanning speed
Level - α	0.9415‰	0.0460‰	0.1545‰
Level -1	0.6451‰	0.4296‰	0.2380‰
Level 0	0.2964‰	0.3745‰	0.3165‰
Level +1	0.1392‰	0.3547‰	0.5463‰
Level + α	0.0392‰	0.2069‰	0.6455‰
Range	0.9024‰	0.3836‰	0.4909‰

material is sprayed into the molten pool, a large laser power can result in a larger molten pool. If the gas does not leave the molten pool in time, bubbles may become trapped. Moreover, the laser power affects the energy density, leading to differences in processing temperature, varied cooling rates, and shortened gas evacuation times, all contributing to pore formation. (3) When the laser power is insufficient, the bond between the material and the substrate will be poor, and the material will not be

completely melted in the substrate so that the unmelted powder particles will be wrapped in it. When the work-piece is cooled, it will be affected by thermal expansion. It will cause cracks, which will cause large-scale faults inside the material.

The scanning speed affects the length of the laser irradiation time per unit area. If the scanning speed is fast, the material will not completely melt and lose energy, and the energy received per unit area will decrease, which will make the material and the substrate bond poorly, resulting in crack. The powder feed rate does not have a direct effect on the porosity. In this study, the method of changing the powder feed rate is to adjust the rotation speed of the powder supply disk, and the gas flow rate of each level is a fixed pressure, so it has no significant impact on the formation of pores.

The variance analysis of each factor is shown in the Table 13; the *F* values of laser power and scanning speed are 20.1256 and 6.3481, which represent that the two control factors are significant factors. And there is an interaction between the three factors. The interaction between the powder feed rate and the scanning speed (BC) is the most significant, because the powder density affects the amount of material entering the molten pool. If there is too much powder material, the powder particles will not be able to receive energy uniformly so that the unmelted powder will be wrapped in it. The interaction between the laser power and the scanning speed (AC) affects the energy density. If the energy density is low, the ability of the molten pool to melt powder will decrease, and the substrate will be heated less, which will make the substrate cool faster, causing more gas to be discharged from the molten pool. This creates bubbles, as shown in Fig. 11.

Fig. 10 Response graph of porosity

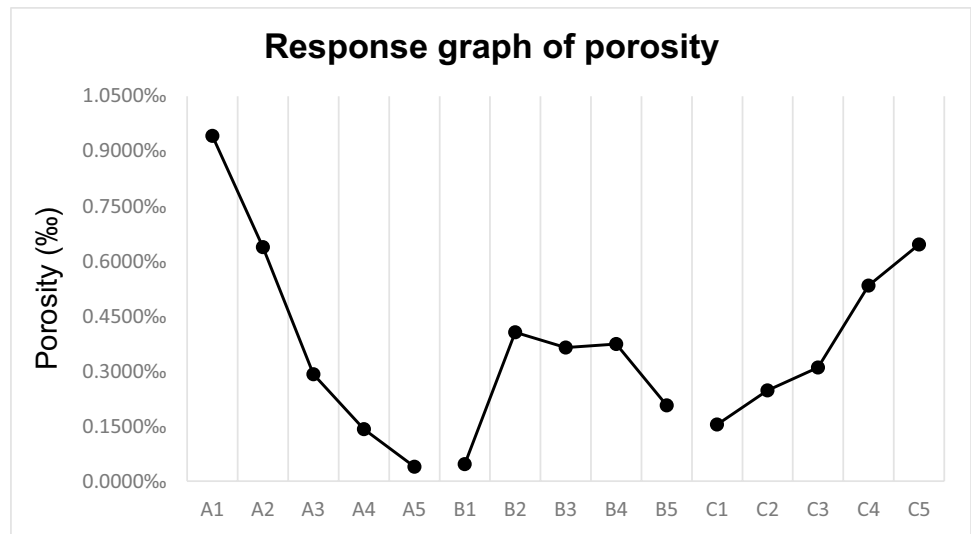


Table 13 ANOVA of porosity

Factor	SS	DF	MS	F value
A	0.89777	1	0.897770	20.1256
B	0.00137	1	0.001370	0.0307
C	0.28318	1	0.283180	6.3481
AB	0.04751	1	0.047510	1.0650
AC	0.06168	1	0.061680	1.3827
BC	0.15430	1	0.154300	3.4590
Error	0.579910	13	0.044608	-
Total	2.02573	19	-	-

3.4 Regression models

Through the factor response graph and ANOVA analysis, the degree of influence of the three factors on product quality was obtained. Then this study established a second-order polynomial regression model to verify the experimental results and establish a parameter prediction model. Since the

units and levels of the three factors are different, each control factor must be normalized before the regression model is established to retain the level distribution of the factors and remove the unit to narrow the value range to [-1, 1]. The following is the numerical normalization calculation equation:

$$U_{Nor_FK} = \frac{U_{FK} - \bar{U}_F}{Max(U_{FK}) - Min(U_{FK})} \in [-1, 1] \quad (11)$$

where U_{Nor_FK} is the normalized value of K level of control factor. U_{FK} is the value before normalization of K level of control factor. \bar{U}_F is the average values of control factor. The comparison table between normalized factors and product quality is shown in the Table 14.

The prediction models of each product quality are shown as below:

$$CE = 0.475 - 0.0511 \cdot A - 0.2667 \cdot B + 0.0376 \cdot C + 0.0333 \cdot A \cdot B + 0.0528 \cdot A \cdot C - 0.1978 \cdot B \cdot C - 0.0654 \cdot A^2 + 0.3541 \cdot B^2 - 0.0086 \cdot C^2 \quad (12)$$

Fig. 11 Image of bubble wrapped in the workpieces (Run 5)

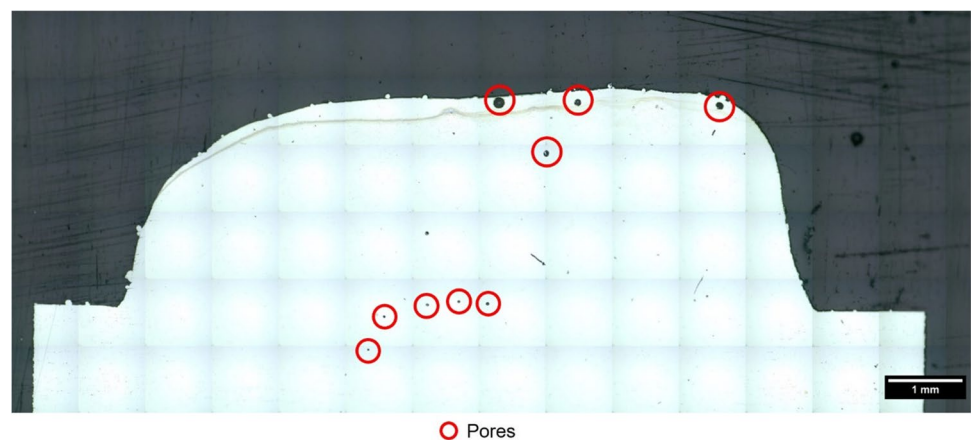


Table 14 Control factor after normalization and measurement result

Run	A Laser power	B Powder feed rate	C Scanning speed	Cladding efficiency (%)	Deposition rate (g/min)	Porosity (‰)
1	-0.5	0	0	44.43%	3.13	1.003‰
2	-0.25	-0.25	-0.25	50.13%	2.53	0.280‰
3	-0.25	0.25	0.25	41.94%	3.80	0.512‰
4	-0.25	0.25	-0.25	41.42%	3.76	0.513‰
5	-0.25	-0.25	0.25	55.17%	2.78	1.274‰
6	0	0	0	48.31%	3.41	0.759‰
7	0	0	0	47.83%	3.38	0.199‰
8	0	0	0	48.80%	3.44	0.272‰
9	0	0	0	46.87%	3.31	0.345‰
10	0	0	0	45.90%	3.24	0.135‰
11	0	0	0	48.31%	3.41	0.141‰
12	0	0	-0.5	47.47%	3.35	0.159‰
13	0	0	0.5	48.11%	3.39	0.686‰
14	0	0.5	0	40.74%	4.52	0.219‰
15	0	-0.5	0	72.98%	2.21	0.045‰
16	0.25	-0.25	0.25	58.79%	2.96	0.151‰
17	0.25	0.25	0.25	45.97%	4.17	0.247‰
18	0.25	0.25	-0.25	44.56%	4.04	0.146‰
19	0.25	-0.25	-0.25	52.01%	2.62	0.012‰
20	0.5	0	0	48.31%	3.41	0.042‰
Avg	-	-	-	48.90%	3.34	0.357‰

$$DR = 3.362 + 0.3689 \cdot A + 2.3764 \cdot B + 0.2155 \cdot C + 0.7457 \cdot A \cdot B + 0.3388 \cdot A \cdot C - 0.8409 \cdot B \cdot C - 0.38 \cdot A^2 - 0.0196 \cdot B^2 + 0.0207 \cdot C^2 \quad (13)$$

$$P_t = 0.132 - 0.9477 \cdot A + 0.0485 \cdot B + 0.5308 \cdot C - 1.2331 \cdot A \cdot B - 1.405 \cdot A \cdot C - 2.2221 \cdot B \cdot C + 0.8043 \cdot A^2 - 0.6512 \cdot B^2 + 0.443 \cdot C^2 \quad (14)$$

The R^2 values of the regression model of cladding efficiency, deposition rate, and porosity are 0.9461, 0.9879, and 0.7887 respectively. This means that the regression model established with the significant control factors of the two qualities as variables has a certain degree of explanatory power. And it can be used as a tool for preliminary prediction of deposition efficiency in the process. The follow-up of this study will analyze the relationship between the experimental results and the prediction model in detail in Chapter 4.

3.5 Optimization of RSM experiments

Since the quality criteria of each product are not the same, the optimal process parameters for each quality are also different. Therefore, in order to obtain optimized parameter combinations for each quality, this study uses Minitab

software for parameter optimization. Before optimization, it is also necessary to normalize each control factor to avoid unification of the optimization standard due to different unit magnitudes. The level of each group of control factors is planned between [-1, 1], as shown in Table 14. The parameter optimization of the response surface method introduced in Section 2.4 is used for calculation. The cladding efficiency and deposition rate are based on the larger-the-best criterion, and the porosity is based on the smaller-the-best criterion.

By optimizing the process parameters through Minitab, the optimal solutions for the three product qualities are obtained, as shown in the Table 15. The laser power is 1800 W, the powder feed rate is 0.8 rpm, and the scanning speed is 12 mm/s. The subsequent Chapter 4 will conduct verification experiments to confirm the correctness of the optimization results.

Table 15 Optimal process parameters calculated by Minitab

Optimization parameters		
A	B	C
Laser power (W)	Powder feed rate (rpm)	Scanning speed (mm/s)
1800	0.8	12

4 Verification experiment and microstructure analysis

4.1 Design of verification experiment

According to the literature review and previous laboratory research results, the optimization of laser power is different from the previous laboratory setting. Considering that in the actual processing process, in order to avoid the overheating of the workpiece and the waste of energy, this study uses a one-factor-at-a-time experiment (OFAT experiment) to fine-tune the laser power. To assess the optimal laser power under identical powder supply and scanning speed conditions and concurrently validate the process parameters determined by Minitab, this study used factor combinations that had been previously validated in the laboratory as controls. The laser power was 1000 W, the powder feed rate was 1.1 rpm, and the scanning speed was 7 mm/s. Similarly, a rectangular block with a length of 25 mm, a width and a height of 8 tracks, and 5 layers is processed for analysis, and the experimental design is shown in the Table 16.

4.2 Results of verification experiment

The verification experiment results are shown in Table 17, where it can be found that the optimized parameters (V2–V6) have been greatly improved compared with the previous process parameters (V1) in the laboratory. Prove that the

parameter optimization experiment results of the response surface experiment method used in this study are correct and effectively optimize product quality. As shown in Fig. 12, compared with the workpieces manufactured by the parameter combination used in the previous laboratory, the V1 workpiece has a large number of pores, and there are a large number of sticky particles on the surface of the workpiece, and the cladding efficiency and porosity are worse than the V3 process. Based on the results of the verification experiment, the V3 process has the best product quality.

The results of the laser power corresponding to the quality of each product are shown from Figs. 13, 14, 15. Through the one-factor-at-a-time experiment, the V3 process parameter combination has the best process quality. Therefore, this study selects the combination of V3 process parameters as the optimal process parameters, including laser power 1700 W, powder feed rate 0.8 rpm, and scanning speed 12 mm/s. The subsequent chapter 5 will use this process parameter to actually manufacture the workpiece product to verify the reliability and practicability of the parameter.

Based on the analysis in the preceding section, this study normalizes the verification experiment data within the range of [-1, 1] and incorporates it into the regression model established in Chapter 3. The objective is to calculate and compare the errors between the predicted values from the experimental model and the actual experimental data, assessing the predictive capability of the regression model.

As shown in Table 18, it can be found that the average error of cladding efficiency between the predicted value

Table 16 Design of verification experiment

<i>Multi-track multi-layer</i>	Run	A Laser power (W)	B Powder feed rate (rpm)	C Scanning speed (mm/s)
Previous setting	V1	1000	1.1	7
Optimized setting by Minitab	V2	1800	0.8	12
OFAT experiment	V3	1700	0.8	12
	V4	1600	0.8	12
	V5	1500	0.8	12
	V6	1400	0.8	12

Table 17 Results of verification experiment

<i>Multi-track multi-layer</i>	Run	Cladding efficiency (%)	Deposition rate (g/min)	Porosity (‰)
Previous setting	V1	30.90%	3.43	1.130‰
Optimized setting by Minitab	V2	49.47%	3.99	0.682‰
OFAT experiment	V3	51.45%	4.15	0.228‰
	V4	48.17%	3.88	0.348‰
	V5	45.82%	3.69	0.508‰
	V6	46.21%	3.73	0.509‰

Fig. 12 Image of cross-section of verification experiment: **a** V1 and **b** V3

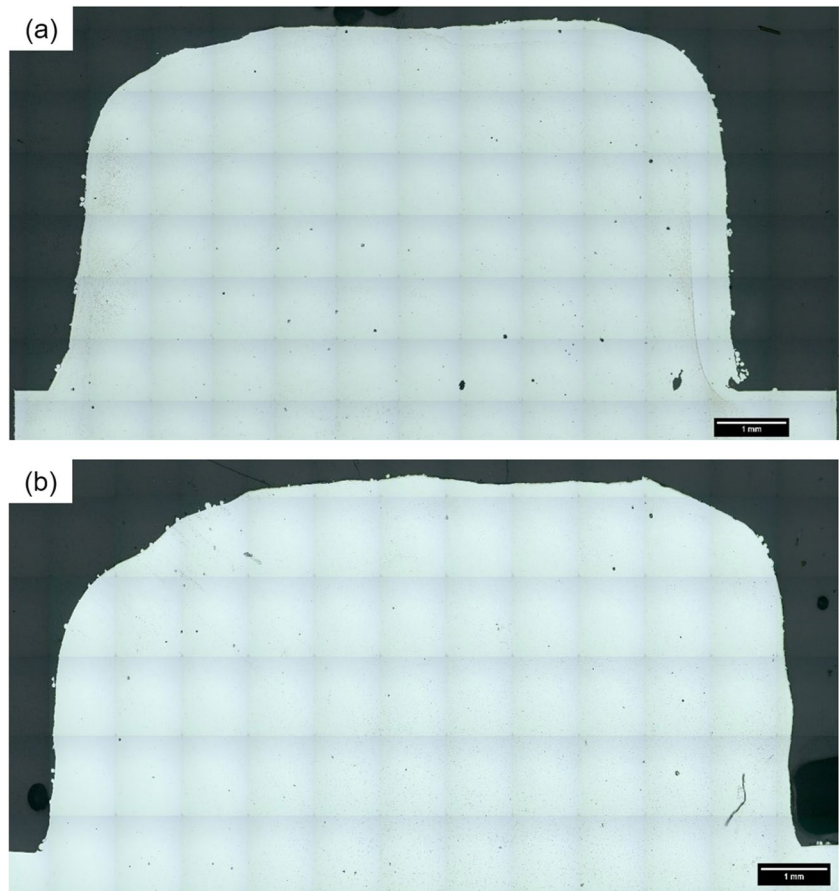
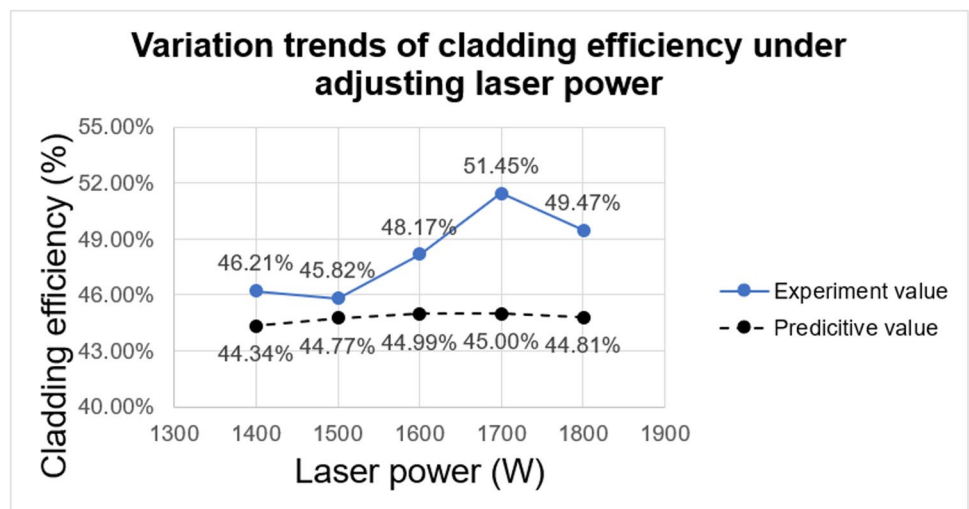


Fig. 13 Variation trends of cladding efficiency under adjusting laser power



and the actual value is 6.98%, indicating that the regression model has excellent quality prediction ability and can be used as one of the methods for predicting product quality before future experiments.

As shown in Table 19, it can be found that the average error of deposition rate between the predicted value and the actual value is 4.94%. And the error value of each group is not

more than 11%. It means that this regression model has excellent quality prediction ability and can be used as one of the methods to predict product quality before future experiments.

As shown in Table 20, it can be found that the average error of porosity between the predicted value and the actual value is 36.1%, which is the highest error among the three regression models. The reason is that

Fig. 14 Variation trends of deposition rate under adjusting laser power

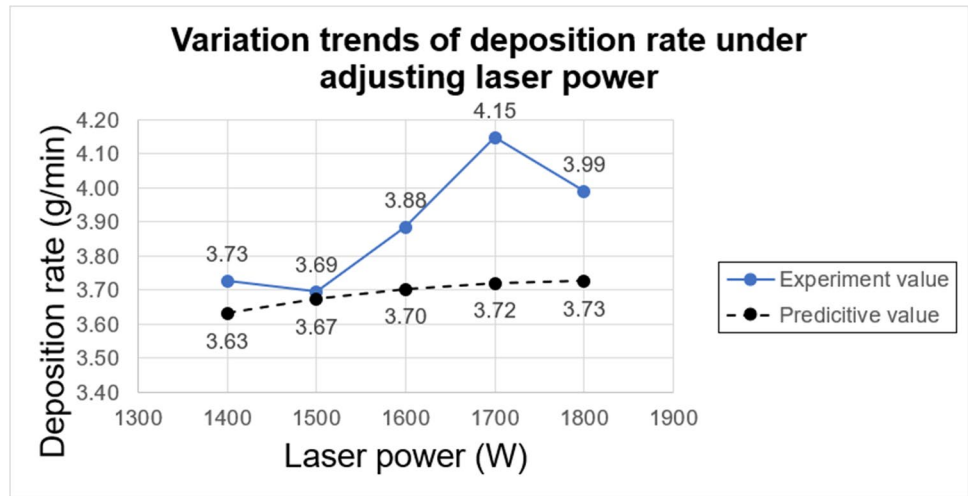


Fig. 15 Variation trends of porosity under adjusting laser power

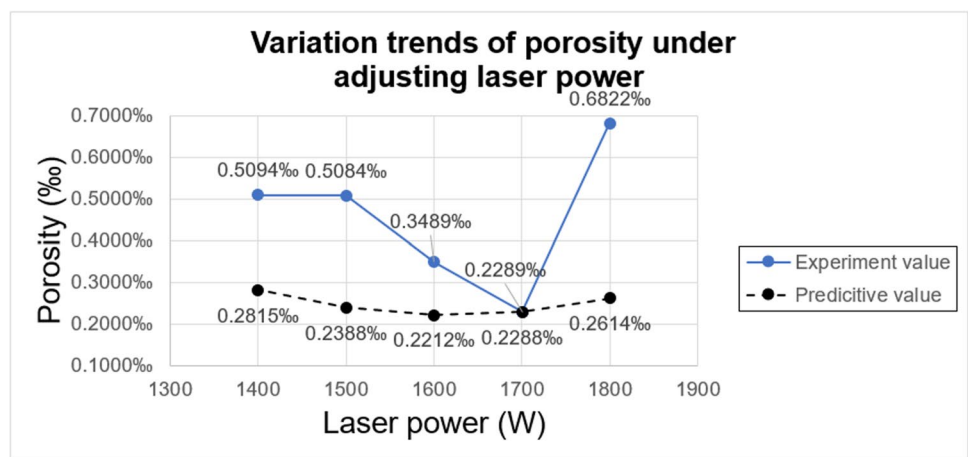


Table 18 Results of cladding efficiency comparison

Multi-track multi-layer	Run	Cladding efficiency (%)		
		Predictive value	Experiment value	Error
Optimized setting by Minitab OFAT experiment	V2	44.81%	49.47%	9.42%
	V3	45.00%	51.45%	12.54%
	V4	44.99%	48.17%	6.60%
	V5	44.77%	45.82%	2.29%
	V6	44.34%	46.21%	4.05%
Previous setting	V1	49.21%	30.90%	59.26%
-	-	-	Avg	6.98%

the porosity is significantly affected by various control factors, and the interaction between factors will affect the porosity, so it is very difficult to accurately predict the porosity. In the past research [15] of our laboratory, the prediction error of porosity reached 358%, and the prediction accuracy was not very satisfactory. The main reason was that the interaction between factors was not considered in the experimental design, so too many interference factors were not calculated. In this study, the

response surface experiment method was used to incorporate the interaction between factors into the calculation. From the research results in Chapter 3, it can be found that there is a significant interaction between the factors. Therefore, when establishing a prediction model, compared with previous studies, the error amount significantly reduced, and the accuracy still reaches 70%, so it can still be used as one of the methods for predicting product quality before the experiment.

Table 19 Results of deposition rate comparison

Multi-track multi-layer	Run	Deposition rate (g/min)		
		Predictive value	Experiment value	Error
Optimized setting by Minitab	V2	3.73	3.99	6.60%
OFAT experiment	V3	3.72	4.15	10.33%
	V4	3.70	3.88	4.67%
	V5	3.67	3.69	0.57%
	V6	3.63	3.73	2.52%
Previous setting	V1	4.69	3.43	36.83%
-	-	-	Avg	4.94%

5 Toolpath planning and parts fabrication

In order to verify the reliability and practicability of the parameters in the above chapters, this study started the research on deposition path planning and manufactured workpieces by verifying the optimal combination of process parameters in experiments. While workpiece modeling, toolpath planning and machine simulation are all carried out on NX CAM software, the version used is NX 1953.

The overall process of this study is summarized as follows: (1) Use CAD to establish workpiece and machine models; (2) use CAM to plan the deposition path; (3) combine the generated workpiece model and path with the machine model for machine simulation verification and correction of tool paths; (4) use post-processing to translate the original path into NC code that can be executed on the machine and add the laser M code customized by the machine; (5) when the laser function is not turned on, run on the machine to confirm that the NC code is correct; (6) turn on the laser function to start making workpieces; and (7) analyze the deposition results. The experiment flow chart is shown in Fig. 16.

5.1 Part geometries

This research intends to establish a nozzle structure. The workpiece has characteristics such as tilting, twisting, and suspension. Therefore, it is necessary to combine five-axis simultaneous machining in manufacturing. According to the research of Shi et al. [16], when three-axis machining is used to manufacture inclined workpieces, there will be a step phenomenon on the surface of the workpiece. When the Inclined angle is too large, the workpiece will collapse. Therefore, it is necessary to carefully calculate the inclination angle during processing. The multi-axis synchronous processing can keep the processing plane perpendicular to the laser head, and there will be no step effect when manufacturing inclined workpieces, and the inclination angle of the workpiece can be larger.

The target workpiece of this research design is shown in the Fig. 17. The workpiece design height is 49 mm, the diameter of the bottom circle is 30 mm, and the diameter of the top circle is 70 mm. The manufacturing parameters used is from the research results in Chapter 4, as shown in the Table 21.

5.2 Toolpath planning

In the DED process, the machining process often responds to different geometric shapes, resulting in the path not being continuous. Therefore, whenever the tool is moved to the next starting point, the machine needs to switch on and off the laser frequently, and the acceleration and deceleration of the starting and ending points also cause depressions or protrusions on the surface of the workpiece. The spiral rising method has continuous processing characteristics. During processing, the initial layer will be deposited for one week, and then the Z-axis height will be raised simultaneously during the deposition process for several weeks, until the preset height and then return to the level for the next week of deposition. This solves the problem of frequent switching of lasers required for the separation of each layer of the

Table 20 Results of porosity comparison

Multi-track multi-layer	Run	Porosity (%)		
		Predictive value	Experiment value	Error
Optimized setting by Minitab	V2	0.2614%	0.6822%	61.68%
OFAT experiment	V3	0.2288%	0.2289%	0.04%
	V4	0.2212%	0.3489%	36.60%
	V5	0.2388%	0.5084%	53.03%
	V6	0.2815%	0.5094%	44.74%
	Previous setting	V1	1.3627%	1.130875%
-	-	-	Avg	36.10%

Fig. 16 Flowchart of toolpath experiment

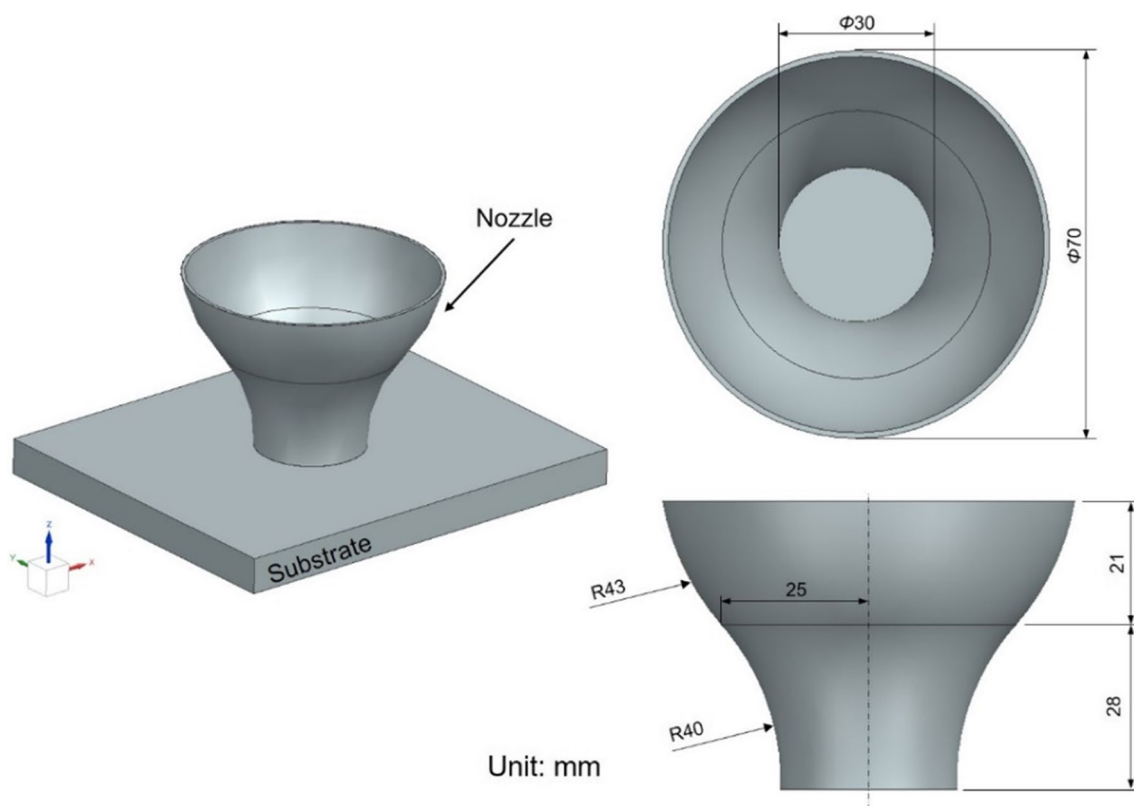
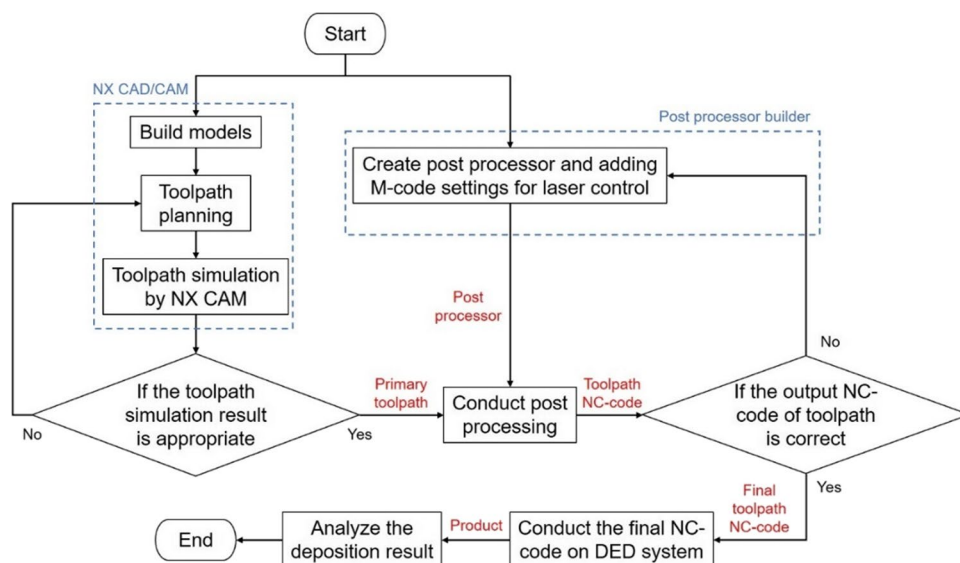


Fig. 17 Schematic of target workpieces (unit: mm)

path. There are no breakpoints in the processing process, and workpieces with relatively flat surfaces and smooth side walls can be manufactured, as shown in the Fig. 18. The target workpiece of this research adopts the “spiral method” as the toolpath planning method.

5.3 Fabrication results of target part

In this study, the optimal combination of process parameters is used. First, a single-track single-layer is produced to obtain the width and height of the single-track

Table 21 Process parameter of toolpath experiment

Process parameters					
Laser power (W)	Overlap ratio (%)	Powder feed rate (rpm)	Scanning speed (mm/s)	Laser defocus (mm)	Z-offset (%)
1700	60	0.8	12	-2	50

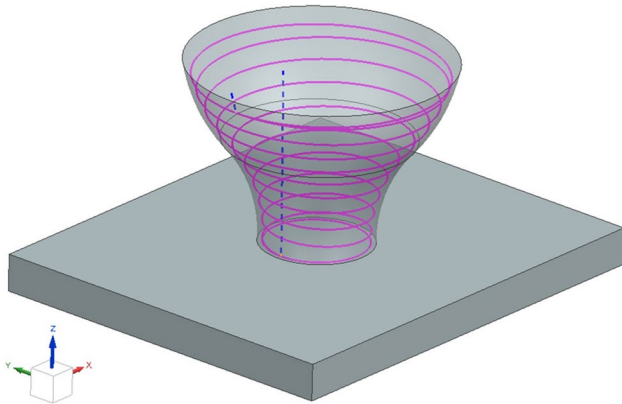


Fig. 18 Schematic of spiral toolpath

of the optimal process parameter combination. The target workpiece processing parameters are set as shown in the Table 22.

The deposition results are shown in the Fig. 19 and Table 23. When the target workpiece is deposited to about 90 layers, the surface of the workpiece begins to collapse obviously, and the height of the workpiece gradually fails to keep up with the design height, resulting in the laser defocus not in the processing position. In the end, subsequent workpieces cannot continue to grow. Therefore, the processing is suspended at the 105 layers.

In this study, the reasons for the deposition failure are summarized as follows:

- (1) By using the spiral rising method, the laser will be turned on during the processing until the five-layer processing is completed, leading to excessive heat accumulation. As a result, thermal shrinkage occurs on the surface of the workpiece, and the deterioration of the surface roughness affects the laser defocus, leading to poor deposition result. The height of the workpiece gradually falls behind the design height until the laser shifts and the deposition fails.

Table 22 The setting of process parameters for fabricating target workpiece

Model	Toolpath planning	Number of layers	Z-offset (%)	Processing time (sec)	Programmed height (mm)
Nozzle_1	Spiral and alternating deposition direction	140	50	2087	36.75

Fig. 19 Image of first toolpath experiment: **a** front view and **b** top view



Table 23 Results of first toolpath experiment

Model	Toolpath planning	Number of layers	Processing time (sec)	Results		
				Cladding efficiency (%)	Deposition rate (g/min)	Measured height (mm)
Nozzle_1	Spiral and alternating deposition direction	105	1353	52.85%	4.26	32.5

Fig. 20 Schematic of deposition height greater than design height

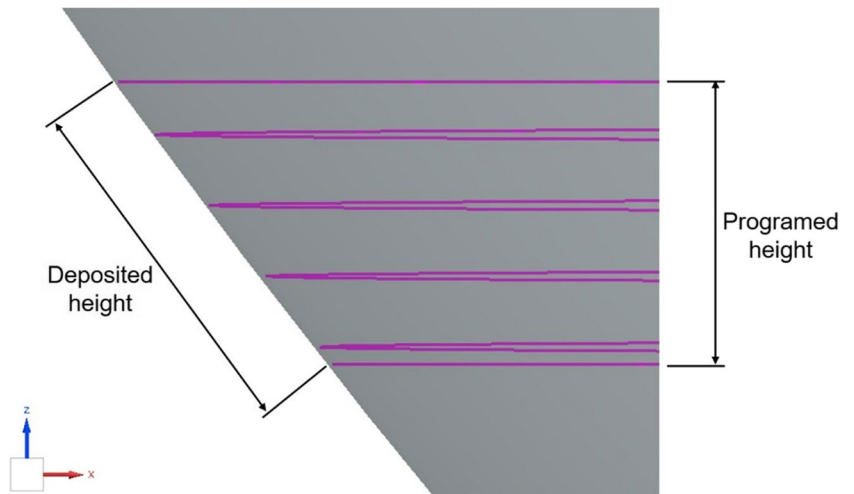
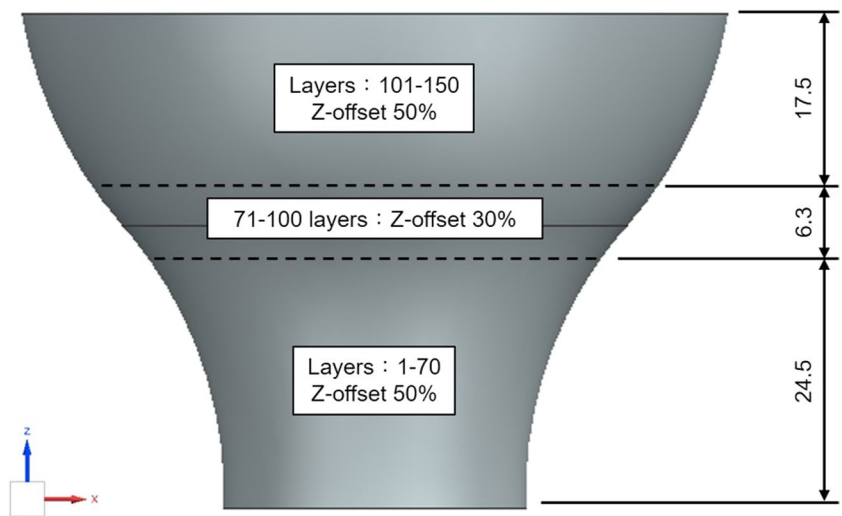


Fig. 21 Schematic of “Mixture Z-offset” setting



(2) Another reason is related to the Z-offset setting. It can be found from the NX software that the designed height of each layer is along the positive Z-axis of the workpiece. However, when processing irregular geometric workpieces with overhangs and twists, the actual deposition height exceeds the design height, as shown in Fig. 20. As a result, the laser head is lifted too much, and the deposition speed of the workpiece cannot keep up with the lifting speed, making the laser gradually defocused.

In order to improve the error of the height setting of the above NX software, in this study, the “Mixture Z-offset”

setting is used to process the target workpiece, as shown in the Fig. 21. The workpiece is manufactured with Z-offset 50% between the 1 layer and the 70 layers. From the 71 layers to the 100 layers, due to the increased overhang angle and twist of the workpiece, the Z-offset is reduced to 30% to ensure that the deposition height is equivalent to the lift height. From the 101 layers to the 150 layers, the Z-offset is restored by 50% to save processing time and material consumption, so as to take into account the cladding efficiency and deposition rate, and at the same time ensure smooth processing of complex geometries. The parameter settings are shown in Table 24.

Table 24 Processing parameter of “Mixture Z-offset”

Model	Toolpath planning	Number of layers	Z-offset (%)	Processing time (sec)	Programmed height (mm)
Nozzle_3	Spiral, Mixture Z-offset	150	50 and 30	2231	48.3

Fig. 22 Image of final toolpath experiment: **a** front view and **b** top view

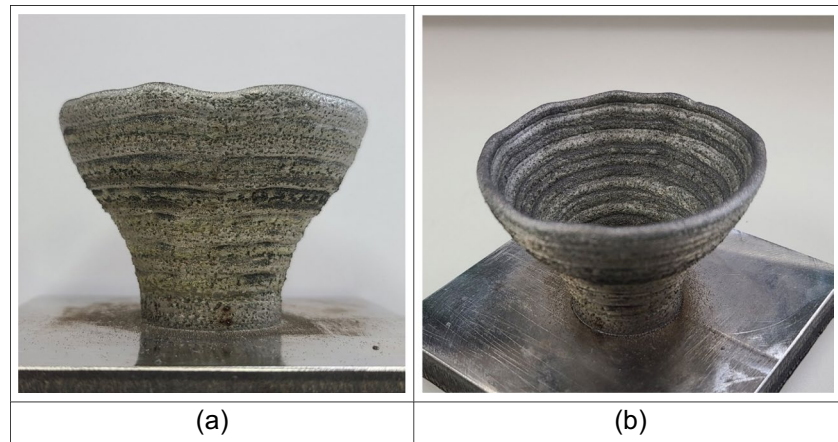


Table 25 Results of final toolpath experiment

Model	Toolpath planning	Number of layers	Processing time (sec)	Weight (g)	Results		
					Cladding efficiency (%)	Deposition rate (g/min)	Measured height (mm)
Nozzle_3	Spiral, Mixture Z-offset	150	2231	201.35	67.15%	5.42	48.65

After improving the engage movement and mixture Z-offset settings, the target workpiece was successfully manufactured. As shown in Fig. 22 and Table 25, the contour of the workpiece is smooth and even, and there are no obvious defects or cracks between layers. The cladding efficiency is 67.15%, and the deposition rate is 5.42 g/min. It proves the reliability and practicability of the optimized process parameter combination in this research, with proper toolpath planning, which can produce high-efficiency and high-quality product workpieces.

6 Conclusion

This study optimized the parameters of the directed energy deposition (DED) process using response surface methodology and central composite design. By analyzing three key process factors, i.e., laser power, powder feed rate, and scanning speed, the following conclusions were drawn:

- (1) Cladding efficiency is primarily influenced by the powder feed rate, while deposition rate is mainly controlled by the powder feed rate, and porosity is primarily regulated by laser power.
- (2) In the analysis of deposition rate as a quality parameter, a significant interaction between powder feed rate and scanning speed is observed. This interaction is primarily attributed to the influence of powder density on the amount of material deposited in the molten pool.

In the analysis of porosity as a quality parameter, a strong interaction between powder feed rate and scanning speed is evident. This is mainly due to an excess of material entering the molten pool, resulting in the entrapment of unmelted powder, which forms pores and leads to an increase in porosity.

- (3) Through regression analysis to establish a quality prediction model. The R^2 values of cladding efficiency, deposition rate, and porosity are 0.9461, 0.9879, and 0.7887 respectively. It represents the predictive model with excellent explanatory power. After verifying the experimental analysis results, the three quality prediction models can effectively predict product quality.
- (4) Utilizing parameter optimization through response surface methodology, we obtained the optimal process parameter combinations for cladding efficiency, deposition rate, and porosity. Following validation experiments, these optimized parameters were applied to actual workpiece manufacturing, confirming their reliability and practicality.
- (5) Through the construction of the nozzle geometry, we validated the reliability of optimized process parameters. Additionally, by improving tool paths and implementing a “mixture Z-offset” machining method, challenges such as starting point collapse and processing steep overhang angles were addressed, providing a solution for manufacturing complex geometries.

Author contribution All authors contributed to the study conception and design. Material preparation, data collection, and analysis were performed by Y.-X.C., Y.-K.H., W.-L.C., and S.-J.H. The first draft of the manuscript was written by J.-R.Q, and all authors commented on previous version of the manuscript. All authors read and approved the final manuscript.

Data availability Not applicable.

Code availability Not applicable.

Declarations

Ethics approval The authors confirm the novelty of the reported work and confirm that it is not submitted to any other journal.

Consent to participate The authors give consent to participate.

Consent to publish The authors give consent for publication.

Conflict of interest The authors declare no competing interests.

References

- Gibson I, Rosen D, Stucker B (2010) Design for additive manufacturing. In: Additive Manufacturing Technologies. Springer, Boston, MA. https://doi.org/10.1007/978-1-4419-1120-9_11
- Guo C, He S, Yue H, Li Q, Hao G (2021) Prediction modelling and process optimization for forming multi-layer cladding structures with laser directed energy deposition. *Opt Laser Technol* 134:106607
- Ansari M, Mohamadizadeh A, Huang Y, Paserin V, Toyserkani E (2019) Laser directed energy deposition of water-atomized iron powder: process optimization and microstructure of single-tracks. *Opt Laser Technol* 112:485–493
- Svetlizky D, Zheng B, Steinberg DM, Schoenung JM, Lavernia EJ, Eliaz N (2022) The influence of laser directed energy deposition (DED) processing parameters for Al5083 studied by central composite design. *J Market Res* 17:3157–3171
- Fujishima M, Oda Y, Ashida R, Takezawa K, Kondo M (2017) Study on factors for pores and cladding shape in the deposition processes of inconel 625 by the directed energy deposition (DED) method. *CIRP J Manuf Sci Technol* 19:200–204
- Ribeiro Kandice S.B., Mariani Fábio E, Coelho Reginaldo T (2020) A study of different deposition strategies in direct energy deposition (DED) processes. *Procedia Manuf* 48:663–670
- Kaji F, Jinoop AN, Zimny M, Frikel G, Tam K, Toyserkani E (2022) Process planning for additive manufacturing of geometries with variable overhang angles using a robotic laser directed energy deposition system. *Additive Manuf Lett* 2:100035
- Oh WJ, Lee WJ, Kim MS, Jeon JB, Shim DS (2019) Repairing additive-manufactured 316L stainless steel using direct energy deposition. *Opt Laser Technol* 117:6–17
- Li L, Zhang X, Liou F (2021) Experimental and numerical investigation in directed energy deposition for component repair. *Materials* 14:1409
- Aydogan B, Sahasrabudhe H (2021) Enabling multi-material structures of co-based superalloy using laser directed energy deposition additive manufacturing. *Metals* 11:1717
- Melzer D, Džugan J, Koukolíková M, Rzepa S, Vavřík J (2021) Structural integrity and mechanical properties of the functionally graded material based on 316L/in718 processed by DED technology. *Mater Sci Eng A* 811:141038
- Wei C, Liu L, Yuchen Gu, Huang Y, Chen Q, Li Z, Li L (2022) Multi-material additive manufacturing of tungsten copper alloy bimetallic structure with a stainless-steel interlayer and associated bonding mechanisms. *Addit Manuf* 50:102574
- Ramiro P, Ortiz M, Alberdi A, Lamikiz A (2020) Geometrical model and strategy in single and multilayer structures deposited by powder-fed Directed Energy Deposition. *Procedia CIRP* 94:352–356
- Derringer G, Suich R (1980) Simultaneous optimization of several response variables. *J Qual Technol* 12:214–219
- Chang YY, Qiu JR, Hwang SJ (2022) Multi-objective optimization of directed energy deposition process by using Taguchi-Grey relational analysis. *Int J Adv Manuf Technol* 120(11–12):7547–7563
- Shi T, Bingheng Lu, Shi S, Meng W, Geyan Fu (2017) Laser metal deposition with spatial variable orientation based on hollow-laser beam with internal powder feeding technology. *Opt Laser Technol* 88:234–241

Publisher's Note Springer Nature remains neutral with regard to jurisdictional claims in published maps and institutional affiliations.

Springer Nature or its licensor (e.g. a society or other partner) holds exclusive rights to this article under a publishing agreement with the author(s) or other rightsholder(s); author self-archiving of the accepted manuscript version of this article is solely governed by the terms of such publishing agreement and applicable law.